# Improving the accuracy of land cover classification in cloud persistent areas using optical and radar satellite image time series

Mailys Lopes[1,2,3], Pierre-Louis Frison[3], Merry Crowson[1], Eleanor Warren-Thomas[4], Bambang Hariyadi[5], Winda D. Kartika[5], Fahmuddin Agus[6], Keith C. Hamer[7], Lindsay Stringer[8], Jane K. Hill[4], and Nathalie Pettorelli[1,*]

[1]Institute of Zoology, Zoological Society of London, Regent's Park, London NW1 4RY, United Kingdom

[2]DYNAFOR, University of Toulouse, INRA, Chemin de Borde Rouge, 31326 Castanet-Tolosan, France

[3]LaSTIG, UPEM/IGN, University Paris-Est Marne-la-Vallée, 5 bd Descartes, 77454 Marne-la-Vallée, France

[4]Department of Biology, University of York, York YO10 5DD, United Kingdom

[5]Biology Education Program, Faculty of Education and Teacher Training, Universitas Jambi, Jl. Raya Jambi-Ma.Bulian km 15 Mendalo Darat, Jambi, Indonesia

[6]Indonesian Soil Research Institute, Indonesian Center for Agricultural Land Resources Research and Development, Jl. Tentara Pelajar No. 12, Cimanggu, Bogor 16114, Indonesia

[7]School of Biology, University of Leeds, Leeds LS2 9JT, United Kingdom

[8]School of Earth and Environment, University of Leeds, Leeds LS2 9JT, United Kingdom

[*]Correspondence author: Nathalie Pettorelli, Institute of Zoology, Zoological Society of London, Regent's Park, London NW1 4RY, United Kingdom, nathalie.petorelli@ioz.ac.uk

**Abstract**

1. The recent availability of high spatial and temporal resolution optical and radar satellite imagery has dramatically increased opportunities for mapping land cover at fine scale. Fusion of optical and radar images has been found useful in tropical areas affected by cloud cover because of their complementarity. However, the multitemporal dimension these data now offer is often neglected because these areas are subject to low seasonality. Therefore, the usefulness of combining optical and radar time series for land cover mapping in these regions has not been assessed.

2. The aim of this work is to test whether land cover classification in tropical areas benefits from optical and radar multitemporal data. We compared the accuracies of classifications based on monotemporal or multitemporal radar data, monotemporal or multitemporal optical data, combination of monotemporal or multitemporal radar and optical data for mapping land cover in Jambi province, Indonesia, using Sentinel-1 and Sentinel-2 images acquired over a year.

3. Combining optical and radar images resulted in significantly higher classification accuracies than optical or radar images alone (Kappa coefficient improvement of +18.3% compared to Sentinel-1 and +10.1% compared to Sentinel-2 for the monotemporal case; +5.6% compared to Sentinel-1 and +9.5% compared to Sentinel-2 for the multitemporal case). Using time series was linked to significantly higher

accuracies than using monotemporal data (+14.7% for Sentinel-1, +2.5% for Sentinel-2 and +2% combining Sentinel-1 and Sentinel-2). Overall, combining Sentinel-2 and Sentinel-1 time series provided the highest accuracies (Kappa = 88.5%).

4. Our study demonstrates that the integration of radar and optical time series in low seasonal environments can significantly improve land cover classifications, improving our capacity to monitor key ecosystems such as peatlands. The proposed method is reproducible, automated, and based on open-source tools satellite imagery.

**Key-words**: cloud persistent areas, fusion, land cover mapping, remote sensing, satellite image time series, Sentinel-1, Sentinel-2

# 1 Introduction

Information on land cover and land cover change is key for ecosystem assessment (Cihlar, 2000). Satellite imagery has become indispensable for producing land cover maps over large areas because of its broad spatial coverage. Together with supervised classification approaches, they enable the automatic production of land cover maps. Up until a few years ago, scientists had access to imagery that was either free of charge but collected at coarse to medium spatial resolution, or at very high resolution but costly, limiting land cover mapping to a low level of detail or restricted spatial coverage. Since 2014, the availability of free satellite imagery combining both high spatial and high temporal resolutions through the Copernicus Programme has dramatically changed what can be mapped from space, increasing opportunities to both detect small elements in the landscapes and capture their seasonal variation, thereby enhancing the definition and the classification of vegetation types (Defourny et al., 2019; Gómez, White, & Wulder, 2016; Lambin & Linderman, 2006; Wulder, Hall, Coops, & Franklin, 2004).

Furthermore, the availability of co-registered optical and radar images through Copernicus facilitates the use of fusion for land cover mapping. Image fusion has often been shown to enhance land cover classification accuracy (Clerici, Calderón, & Posada, 2017; Inglada, Vincent, Arias, & Marais-Sicre, 2016; Joshi et al., 2016; Van Tricht, Gobin, Gilliams, & Piccard, 2018) because the information captured by optical and radar sensors is fundamentally different and thus complementary (Kasischke, Melack, & Dobson, 1997). In tropical and boreal areas, optical data availability is often limited by cloud cover leading to radar data being preferred map land cover in these regions (Asner, 2001; Hoekman, Vissers, & Wielaard, 2010; Kasischke et al., 1997).

Interestingly, the information captured by high temporal resolution sensors has often been neglected in tropical environments, mainly because of the low level of seasonality characterising many of these ecosystems. Therefore, most land cover maps generated for these regions are based on single-date or cloud-free composites (i.e., Crowson et al., 2018; Erinjery, Singh, & Kent, 2018). Cloud-free composites can, however, be difficult and time-consuming to build. Similarly, the multitemporal dimension is often overlooked when fusing optical

and radar data, mostly because of the unavailability of radar time series before the launch of Sentinel-1 in 2014. Hence, the utility of fusing optical and radar multitemporal satellite images for land cover mapping has hardly ever been assessed (Hirschmugl, Sobe, Deutscher, & Schardt, 2018; Inglada et al., 2016; Kuenzer et al., 2014); to our knowledge, this type of approach has never been considered in tropical regions with persistent cloud cover and limited seasonality. The aim of this study is to fill this gap by assessing the accuracy of approaches combining optical (Sentinel-2) and radar (Sentinel-1) intra-annual time series to map land cover in tropical regions affected by dense cloud cover, focusing on peatlands in the Jambi province, Indonesia, as part of a collaborative UK – Indonesia research project.

Tropical peatlands are very important for carbon storage and are biodiversity hotspots (Wijedasa et al., 2017). Peatland forests have been heavily degraded around the world through deforestation and drainage to make land available for agriculture, leading to carbon release and severe and damaging fires (Miettinen, Shi, & Liew, 2012; Posa, Wijedasa, & Corlett, 2011; Wijedasa et al., 2017). Efforts to restore degraded peatlands – which are part of Sustainable Development Goals – have recently been made in Indonesia, where most of Southeast Asia's peatlands are located (van Eijk, Leenman, Wibisono, & Giesen, 2009). Accurately monitoring land cover in the humid tropics, such as in the context of restoration efforts in tropical peatlands, is critical to ensure effective conservation and restoration action, and to inform ongoing policies and strategies.

Here we test four hypotheses concerning the accuracy of land cover classification in cloud persistent areas using monotemporal and multitemporal data in the optical and radar domains. As our study site is characterised by a low seasonality, the use of time series (multitemporal data) should have a limited impact on land cover map accuracy compared to using a single date (monotemporal) approach (H1). Consequently, the fusion of optical and radar time series should have an equivalent classification accuracy to the fusion of a single date optical image and a single date radar image (H2). Based on the assumption that optical and radar data offer complementary information, we expect that the fusion of an optical image and a radar image will improve classification accuracy compared to using an optical image only or a radar image only (H3). Based on the same assumption, the use of combined optical and radar time series is expected to improve classification accuracy compared to optical times series or radar time series alone (H4).

# 2 Materials and Methods

## 2.1 Study area

The study area is located along the eastern coast of Jambi province in Sumatra (Indonesia, Fig. 1). It covers an area of 12,710 $km^2$ that is mostly flat. The climate is tropical humid, with an average annual precipitation of 2,400 mm (Hapsari et al., 2017). Even during the dry season (June to September), monthly precipitation is above 100 mm, meaning the region is primarily subject to low seasonality (Aldrian & Susanto, 2003; Crowson

et al., 2018; Karger et al., 2016).

The study area comprises both anthropogenic environments (agriculture, urban areas) and natural vegetation (peat swamp forest, mineral soil lowland rainforest, mangrove). It is mainly dominated by plantations (oil palm, coconut palm, areca palm, acacia, rubber) that have replaced forests as large monoculture or smallholder plantations. The eastern part of the study area is dominated by Berbak National Park (about 1,850 $km^2$), which is a protected (IUCN category II), undrained peat swamp forest that supports plant and animal biodiversity (Giesen, 2004). The forest is surrounded by fern-dominated scrublands which are regrowth areas left unmanaged after severe fires. The Sungai Buloh Forest Reserve is located in the central part of the study area and covers an area of about 120 $km^2$. Mangroves are primarily found along the coast.

## 2.2 Reference data

Reference data were generated through visual interpretation of very high spatial resolution images (2017 Google Earth imagery and 2017 PlanetScope scenes), itself informed by field visits around the Sungai Buloh Forest. We primarily used the same classes as Crowson et al. (2018), namely peat swamp forest, water, urban, palm trees (all combined), acacia trees, fern/scrublands, bare ground; only a mangrove class was added to this original list. Mangrove polygons were digitized using the USGS Global distribution of mangroves (`http://data.unep-wcmc.org/datasets/4`). In total, reference data comprised 1399 polygons distributed in 8 classes, representing about 1.5 millions pixels (1.2% of the study area).

## 2.3 Satellite imagery

### 2.3.1 Sentinel-2

We used optical images acquired by Sentinel-2 along two different orbit paths to cover the whole study area (7 tiles in total). We downloaded all the images acquired in 2017 presenting a maximum of 70% cloud cover ; this resulted in 10 to 12 dates per tile. The Level L1C images (orthorectified and radiometrically corrected to Top of Atmosphere reflectance) were processed to Level L2A surface reflectances (corrected for atmospheric effects and slope effects) using the Sen2Cor processor (version 2.5.5) (`http://step.esa.int/main/third-party-plugins-2/sen2cor/sen2cor_v2-5-5/`). The algorithm provides a scene classification including pixels affected by noise such as clouds and cloud shadows. Those pixels were masked and filled using a temporal gap-filling method (*Image Time Series Gap Filling* application from the Orfeo ToolBox ; OTB (Grizonnet et al., 2017)) that replaces the masked/invalid pixels with a value interpolated from the valid dates of the time series. During this process, the time series of each tile were also resampled to the same temporal grid to facilitate the subsequent mosaicking. The temporal grid was chosen based on the original 10 temporal acquisitions of the main (central) tile of the study area. In the end, all the pixels of the study area

had the same dates: 2017-02-20, 2017-03-12, 2017-07-10, 2017-07-25, 2017-07-30, 2017-08-19, 2017-10-08, 2017-10-18, 2017-11-22, 2017-12-22. This temporal gap-filling process was done for each of the ten Sentinel-2 spectral bands at spatial resolutions of 10m and 20m (resampled to 10m resolution using a nearest neighbor interpolation). Finally, the tiles from the two orbits were mosaicked using a mosaic technique from the OTB application (`https://github.com/remicres/otb-mosaic`) that blends all the images on the overlapping areas, resulting in a seamless unique raster covering the whole study area.

Because of the unavailability of cloud-free acquisitions for this study area, we computed the annual temporal average from the gap-filled time series and used it as our single date/monotemporal approach to test H1-3.

### 2.3.2 Sentinel-1

Since radar images are not affected by cloud cover, all the Sentinel-1 images acquired between February and December 2017 over the study area were used to match the temporal coverage of the optical time series. In total, there were 26 images, acquired every 12 days from 2017-02-03 to 2017-12-24. The images were acquired over the same orbit, so no mosaicking was necessary. The Level-1 Ground Range Detected High Resolution (GRDH) were radiometrically calibrated to the radar backscattering coefficient $\sigma^0$ for both polarizations VV and VH using OTB application *SAR Radiometric Calibration* (Laur et al., 2004). They were then orthorectified to correct for the geometric distortions using the OTB application *OrthoRectification* (Small & Schubert, 2008). The output spatial resolution was 10m per pixel. The images were subsequently converted from intensity to the logarithm dB scale, and the ratio VH/VV was computed as a third polarization.

Finally, the speckle effects, inherent to radar data, must be filtered to reduce the noise in the image. For the single date/monotemporal approach, we computed the annual temporal average from the time series that resulted in an image with reduced speckle effects (Zhao, 2019). For the time series/multitemporal approach, the speckle effects were reduced with a temporal filter (Quegan & Yu, 2001) that does not degrade the spatial resolution (Trouvé, Chambenoit, Classeau, & Bolon, 2003).

## 2.4 Classification protocol

The classification was performed using Random Forest (RF), one of the fastest algorithms for pixel-based classification with a large number of pixels and variables (Breiman, 2001; Pelletier, Valero, Inglada, Champion, & Dedieu, 2016). We used RF implemented in OTB applications with the following parameters: maximum depth of tree = 25; minimum number of samples in each node = 25; maximum number of trees in the forest = 100. The reference dataset was split randomly into disjoint training (75%) and validating (25%) subsets. The split was performed at the polygon level in order to ensure an independent set of pixels between the training and the validation steps (i.e., no pixels belonging to the same polygon in the training and validating

subsets). The resulting classification maps were sieved to eliminate isolated pixels and thus to reduce the 'salt and pepper' effect associated with a pixel-based classification. Finally, the accuracy of the produced land cover maps was assessed by computing the confusion matrix based on the validation subset and by extracting accuracy metrics (Kappa coefficient, User's accuracy, Producer's accuracy).

Six land cover classifications based on six different inputs were tested and compared:

- $S1_a$: annual temporal average of Sentinel-1 images in the 3 polarizations (monotemporal radar case),
- $S1_t$: Sentinel-1 time series in the 3 polarizations (multitemporal radar case),
- $S2_a$: annual temporal average of Sentinel-2 in the 10 spectral bands (monotemporal optical case),
- $S2_t$: Sentinel-2 time series in the 10 spectral bands (multitemporal optical case),
- $S1_a$+$S2_a$: the combination of Sentinel-1 and Sentinel-2 annual temporal averages (fusion of radar and optical monotemporal images)
- $S1_t$+$S2_t$: the combination of Sentinel-1 and Sentinel-2 time series (fusion of radar and optical multi-temporal images).

For the latter two in the list above, the combination was performed by stacking both annual temporal averages / time series prior to classification.

Additionally, an *a posteriori* fusion of classifications based on Sentinel-2 and Sentinel-1 was performed to account for undetected clouds by the cloud-masking algorithm. We therefore added a supplementary "cloud" class to the classifications based on Sentinel-2 data (by adding non-detected clouds polygons in the training dataset), so that areas of permanent non-detected cloud cover could be identified. Then, the pixels tagged as "clouds" in the subsequent classification were replaced with the results of the classification obtained with Sentinel-1. The outcomes of this *a posteriori* classification are only presented for the $S1_t$+$S2_t$ classification (named "$S1_t$+$S2_t$ fused $S1_t$").

Kappa coefficients associated with each pair of confusion matrices were compared to identify possible significant differences in accuracies associated with our six land cover classifications (Congalton & Green, 1998). The test statistic $Z$ was assessed as follows:

$$Z = \frac{|K_1 - K_2|}{\sqrt{\sigma_1^2 - \sigma_2^2}}$$

where $K_i$ is the Kappa coefficient resulting from the $i^{\text{th}}$ confusion matrix and $\sigma_i$ is the large sample variance of $K_i$ (see Congalton & Green, 1998).

The workflow of the preprocessing of the images and of the classification process can be found in Fig. 2.

# 3 Results

Contrary to our first expectation (H1), using the optical or radar time series resulted in significantly ($P$-value $< 0.001$) higher Kappa coefficient than using their temporal average counterparts (82.9% for $S1_t$ against 68.2% for $S1_a$ and 79.0% for $S2_t$ against 76.5% for $S2_a$). Similarly, using the fusion of optical and radar time series improved significantly ($P$-value $< 0.001$) the land cover classification compared to using the fusion of optical and radar temporal averages (from Kappa = 86.6% for $S1_a$+$S2_a$ to Kappa = 88.5% for $S1_t$+$S2_t$), contradicting our second hypothesis (H2).

Our results however support our third and fourth hypotheses. Specifically, combining the temporal averages of Sentinel-1 and Sentinel-2 significantly ($P$-value $< 0.001$) improved the classification accuracy (Kappa = 86.6% for $S1_a$+$S2_a$) compared to using Sentinel-1 temporal average only (Kappa = 68.2%, $S1_a$) or Sentinel-2 temporal average only (Kappa = 76.5%, $S2_a$) (H3). Similarly, combining times series of optical and radar data significantly ($P$-value $< 0.001$) improved the classification accuracy (Kappa = 88.5% $S1_t$+$S2_t$, see maps in Fig. 3) compared to time series of optical data alone (Kappa = 79.0%, $S2_t$) or time series of radar data alone (Kappa = 82.9%, $S1_t$) (H4). These results are summarized in Table 1.

Overall, the best classification accuracy was obtained when replacing pixels identified as clouds by the classifier using $S1_t$+$S2_t$ (Fig. 4, top) with results from $S1_t$ classification: the Kappa coefficient reached 89.4% ($S1_t$+$S2_t$ fused $S1_t$, Fig. 4, bottom), significantly ($P$-value $< 0.001$) improving by 1% the accuracy of the $S1_t$+$S2_t$ classification.

# 4 Discussion

Our results demonstrate for the first time the usefulness of combining optical and radar time series to map land cover in regions with persistent cloud cover. Despite the low seasonality characterising these environments, using multitemporal images significantly improved the discrimination between vegetation classes compared to using annual temporal averages, suggesting that seasonal differences occur among classes and should not be neglected. Combining optical and radar images also significantly improved the land cover classification, with radar data nicely complementing optical data in clouded areas.

The proposed method can easily be applied to large areas and reproduced in other regions because it is based on freely-accessible satellite imagery and all the steps can be processed automatically in a processing chain reliant on open-source software tools. Unlike previous attempts to map peat land cover in the region creating a manual cloud-free composite (see e.g. Crowson et al. (2018)), no manual inputs are required (except to form the reference dataset, including persistent cloud cover polygons, but this step is essential to all supervised classifications) ; the proposed method is thus time-saving and less sensitive to human errors.

To our surprise, the accuracy of the classification based on radar time series was 4% higher than the

classification based on optical time series. Interestingly, however, more accurate classifications are not systematically generate "better" maps. First, maps derived from radar data are riddled with noise due to the speckle effect that is typically associated with radar imagery; although filtered, this effect was still present in our classification and led to numerous misclassified pixels (Fig. 3, top). An additional filter could be applied to reduce this effect but it would be at the cost of spatial resolution, losing details such as drainage channels. Second, Sentinel-1 data tend to confuse palm trees and mangroves with peat swamp forest, leading to an overestimation of peat swamp forest cover (Fig.3, top). Surprisingly, mangroves were not well identified using this sensor (see per-class accuracies in Table 2 in the Supporting Information). The main difference between mangroves and peat swamp forest is that mangroves are submerged by sea water all year long (Wikramanayake, Dinerstein, Loucks, & Pimm, 2002). Radar data are sensitive to soil wetness and were therefore expected to capture this difference well (Kasischke et al., 1997); the issue here, however, is that canopy cover is very dense, meaning that Sentinel-1 C-band might not have been able to penetrate it. Li, Lu, Moran, Dutra, and Batistella (2012) found that L-band provides much better accuracy than C-band for land cover mapping in tropical moist regions. However, neither of them could separate the types of forests investigated, showing the unsuitability of radar data alone to accurately map the very similar vegetation classes found in their study area. In our study, Sentinel-2 was much better at discriminating between mangrove and peat swamp forest than Sentinel-1. Similar results were found by Erinjery et al. (2018) using Sentinel-2 & -1 to map vegetation in a tropical rainforest.

The use of optical data in regions affected by persistent cloud cover, even as part of the fusion of optical and radar data, nevertheless raises technical issues. When areas particularly affected by cloud cover are detected, they can be automatically masked and complemented by radar data. In our case, however, many clouds were not detected by our chosen cloud detector algorithm, which caused important problems in the classification process. Specifically, the training of the classifier was made on a dataset that included "cloudy" Sentinel-2 pixels associated with various land cover categories, which ultimately reduced separability between classes. When looking at the generated land cover map, it resulted in holes in the land covers (for instance palm tree pixels in the middle of the forest, see Fig. 3, middle and bottom). To overcome this issue, we had to add a supplementary class "clouds" in the classification involving Sentinel-2 data to identify these rogue areas. Although requiring additional steps in our overall classification process (Fig. 2), this approach allowed us to better detect clouds and produced the most accurate land cover map (Fig. 4, bottom).

Altogether, this work demonstrates how the combination of recent algorithmic advances in big data processing and new earth observation capabilities associated with the development of the Copernicus programme has the potential to significantly improve our ability to monitor key ecosystems in remote regions. Combining optical and radar time series indeed resulted in higher accuracies for the mapping of peat swamp forests, allowing environmental managers and policy makers to access up-to-date, fine scale information about peat-

land distribution, thereby supporting efforts to protect and restore these ecosystems. Combining optical and radar time series to map land cover can seem daunting to ecologists used to classifying single optical images; however, recent computational advances as well as existing spatial compatibilities between Sentinel-1 and Sentinel-2 imagery significantly improve the accessibility of such approaches, and our work clearly demonstrates that efforts to go beyond classical approaches do pay off. We therefore urge scientists and practitioners to start exploiting the full capacity of Sentinel-2 and Sentinel-1 to monitor sensitive habitats in areas of conservation interest.

## Acknowledgements

This publication has been written with the support of the AgreenSkills+ fellowship programme which has received funding from the EU's Seventh Framework Programme under grant agreement N°FP7-609398 (AgreenSkills+ contract); the Toulouse-INP international mobility grant (SMI); and the Newton Fund project "Enhancing the benefits of tropical peatland restoration for supporting local communities and ecosystem processes", NERC Reference: NE/P014658/1.

## Authors' contributions

ML, PLF and NP conceived the ideas and designed the methodology; BH, WDK, MC and EWT collected the reference data with the help of FA; ML performed the image processing and the analysis; ML wrote the manuscript with feedback from NP, PLF, MC, EWT, JKH, FA, KCH and LS. All authors contributed critically to the drafts and gave final approval for publication.

## Data Availability

The satellite images used in this study can be downloaded in the Copernicus Open Access Hub (`https://scihub.copernicus.eu/dhus/`). The images can be processed using the Orfeo ToolBox open-source software that can be downloaded at `https://www.orfeo-toolbox.org`.

# References


Aldrian, E., & Susanto, R. D. (2003). Identification of three dominant rainfall regions within Indonesia and their relationship to sea surface temperature. *International Journal of Climatology*, *23*(12), 1435-1452. doi: 10.1002/joc.950

Asner, G. P. (2001). Cloud cover in Landsat observations of the Brazilian Amazon. *International Journal of Remote Sensing*, *22*(18), 3855-3862. doi: 10.1080/01431160010006926

Breiman, L. (2001). Random forests. *Machine Learning*, *45*(1), 5–32.

Cihlar, J. (2000). Land cover mapping of large areas from satellites: Status and research priorities. *International Journal of Remote Sensing*, *21*(6-7), 1093-1114. doi: 10.1080/014311600210092

Clerici, N., Calderón, C. A. V., & Posada, J. M. (2017). Fusion of Sentinel-1A and Sentinel-2A data for land cover mapping: a case study in the lower Magdalena region, Colombia. *Journal of Maps*, *13*(2), 718-726. doi: 10.1080/17445647.2017.1372316

Congalton, R., & Green, K. (1998). *Assessing the accuracy of remotely sensed data: Principles and practices*. CRC-Press.

Crowson, M., Warren-Thomas, E., Hill, J. K., Hariyadi, B., Agus, F., Saad, A., ... Pettorelli, N. (2018). A comparison of satellite remote sensing data fusion methods to map peat swamp forest loss in Sumatra, Indonesia. *Remote Sensing in Ecology and Conservation*. doi: 10.1002/rse2.102

Defourny, P., Bontemps, S., Bellemans, N., Cara, C., Dedieu, G., Guzzonato, E., ... Koetz, B. (2019). Near real-time agriculture monitoring at national scale at parcel resolution: Performance assessment of the Sen2-Agri automated system in various cropping systems around the world. *Remote Sensing of Environment*, *221*, 551 - 568. doi: https://doi.org/10.1016/j.rse.2018.11.007

Erinjery, J. J., Singh, M., & Kent, R. (2018). Mapping and assessment of vegetation types in the tropical rainforests of the Western Ghats using multispectral Sentinel-2 and SAR Sentinel-1 satellite imagery. *Remote Sensing of Environment*, *216*, 345 - 354. doi: https://doi.org/10.1016/j.rse.2018.07.006

Giesen, W. (2004). *Causes of peat swamp forest degradation in Berbak NP, Indonesia, and recommendations for restoration* (Tech. Rep.). ARCADIS Euroconsult. doi: 10.13140/RG.2.2.16544.64006

Grizonnet, M., Michel, J., Poughon, V., Inglada, J., Savinaud, M., & Cresson, R. (2017). Orfeo ToolBox: open source processing of remote sensing images. *Open Geospatial Data, Software and Standards*, *2*(1), 15. doi: 10.1186/s40965-017-0031-6

Gómez, C., White, J. C., & Wulder, M. A. (2016). Optical remotely sensed time series data for land cover classification: A review. *ISPRS Journal of Photogrammetry and Remote Sensing*, *116*, 55 - 72. doi: https://doi.org/10.1016/j.isprsjprs.2016.03.008

Hapsari, K. A., Biagioni, S., Jennerjahn, T. C., Reimer, P. M., Saad, A., Achnopha, Y., ... Behling, H. (2017). Environmental dynamics and carbon accumulation rate of a tropical peatland in Central Sumatra, Indonesia. *Quaternary Science Reviews*, *169*, 173 - 187. doi: https://doi.org/10.1016/j.quascirev.2017.05.026

Hirschmugl, M., Sobe, C., Deutscher, J., & Schardt, M. (2018). Combined use of optical and synthetic aperture radar data for REDD+ applications in Malawi. *Land*, *7*(4). doi: 10.3390/land7040116

Hoekman, D. H., Vissers, M. A. M., & Wielaard, N. (2010). PALSAR wide-area mapping of Borneo: Methodology and map validation. *IEEE Journal of Selected Topics in Applied Earth Observations and Remote Sensing*, *3*(4), 605-617. doi: 10.1109/JSTARS.2010.2070059

Inglada, J., Vincent, A., Arias, M., & Marais-Sicre, C. (2016). Improved Early Crop Type Identification By Joint Use of High Temporal Resolution SAR And Optical Image Time Series. *Remote Sensing*, *8*(5). Retrieved from `https://www.mdpi.com/2072-4292/8/5/362` doi: 10.3390/rs8050362

Joshi, N., Baumann, M., Ehammer, A., Fensholt, R., Grogan, K., Hostert, P., ... Waske, B. (2016). A review of the application of optical and radar remote sensing data fusion to land use mapping and monitoring. *Remote Sensing*, *8*(1).

Karger, D. N., Conrad, O., Böhner, J., Kawohl, T., Kreft, H., Soria-Auza, R. W., ... Kessler, M. (2016). *CHELSA climatologies at high resolution for the earth's land surface areas (Version 1.1).* World Data Center for Climate (WDCC) at DKRZ. doi: 10.1594/WDCC/CHELSA_v1_1

Kasischke, E. S., Melack, J. M., & Dobson, M. C. (1997). The use of imaging radars for ecological applications—a review. *Remote Sensing of Environment*, *59*(2), 141 - 156. doi: https://doi.org/10.1016/S0034-4257(96)00148-4

Kuenzer, C., Ottinger, M., Wegmann, M., Guo, H., Wang, C., Zhang, J., ... Wikelski, M. (2014). Earth observation satellite sensors for biodiversity monitoring: potentials and bottlenecks. *International Journal of Remote Sensing*, *35*(18), 6599-6647. doi: 10.1080/01431161.2014.964349

Lambin, E. F., & Linderman, M. (2006). Time series of remote sensing data for land change science. *IEEE Transactions on Geoscience and Remote Sensing*, *44*(7), 1926-1928. doi: 10.1109/TGRS.2006.872932

Laur, H., Bally, P., Meadows, P., Sanchez, J., Schaettler, B., Lopinto, E., & Esteban, D. (2004). *Derivation of the backscattering coefficient $\sigma o$ in ESA ERS SAR PRI products* (Calibration/Validation Document Nos. Issue 2, Rev. 5f). ESA.

Li, G., Lu, D., Moran, E., Dutra, L., & Batistella, M. (2012). A comparative analysis of ALOS PALSAR L-band and RADARSAT-2 C-band data for land-cover classification in a tropical moist region. *ISPRS Journal of Photogrammetry and Remote Sensing*, *70*, 26 - 38. doi: https://doi.org/10.1016/j.isprsjprs.2012.03.010

Miettinen, J., Shi, C., & Liew, S. C. (2012). Two decades of destruction in Southeast Asia's peat swamp forests. *Frontiers in Ecology and the Environment*, *10*(3), 124-128. doi: 10.1890/100236

Pelletier, C., Valero, S., Inglada, J., Champion, N., & Dedieu, G. (2016). Assessing the robustness of random forests to map land cover with high resolution satellite image time series over large areas. *Remote Sensing of Environment*, *187*, 156 - 168. doi: https://doi.org/10.1016/j.rse.2016.10.010

Posa, M. R. C., Wijedasa, L. S., & Corlett, R. T. (2011). Biodiversity and Conservation of Tropical Peat Swamp Forests. *BioScience*, *61*(1), 49-57. doi: 10.1525/bio.2011.61.1.10

Quegan, S., & Yu, J. J. (2001). Filtering of multichannel SAR images. *IEEE Transactions on Geoscience and Remote Sensing*, *39*(11), 2373-2379. doi: 10.1109/36.964973

Small, D., & Schubert, A. (2008). Guide to ASAR geocoding. *ESA-ESRIN Technical Note RSL-ASAR-GC-AD*, *1*.

Trouvé, E., Chambenoit, Y., Classeau, N., & Bolon, P. (2003). Statistical and operational performance assessment of multitemporal SAR image filtering. *IEEE Transactions on Geoscience and Remote Sensing*, *41*(11), 2519-2530. doi: 10.1109/TGRS.2003.817270

van Eijk, P., Leenman, P., Wibisono, I. T., & Giesen, W. (2009). Regeneration and restoration of degraded peat swamp forest in Berbak NP, Jambi, Sumatra, Indonesia. *Malayan Nature Journal*, *61*, 223-241.

Van Tricht, K., Gobin, A., Gilliams, S., & Piccard, I. (2018). Synergistic Use of Radar Sentinel-1 and Optical Sentinel-2 Imagery for Crop Mapping: A Case Study for Belgium. *Remote Sensing*, *10*(10). doi: 10.3390/rs10101642

Wijedasa, L. S., Jauhiainen, J., Könönen, M., Lampela, M., Vasander, H., Leblanc, M.-C., ... Andersen, R. (2017). Denial of long-term issues with agriculture on tropical peatlands will have devastating consequences. *Global Change Biology*, *23*(3), 977-982. doi: 10.1111/gcb.13516

Wikramanayake, E., Dinerstein, E., Loucks, C., & Pimm, S. (2002). *Terrestrial ecoregions of the indo-pacific: A conservation assessment*. Island Press.

Wulder, M. A., Hall, R. J., Coops, N. C., & Franklin, S. E. (2004). High Spatial Resolution Remotely Sensed Data for Ecosystem Characterization. *BioScience*, *54*(6), 511-521. doi: 10.1641/0006-3568(2004)054[0511:HSRRSD]2.0.CO;2

Zhao, W. (2019). *Multitemporal SAR images denoising and change detection : applications to Sentinel-1 data* (Thesis). Université Paris-Saclay.

# Tables

Table 1: Hypotheses and their results.

| Name | Statement | Results | Conclusion |
|---|---|---|---|
| H1 | Time series and monotemporal image approach result in equivalent classification accuracy. | $S1_t > S1_a$; $S2_t > S2_a$ | Not verified. |
| H2 | Fusion of optical and radar time series and fusion of monotemporal optical and radar images result in equivalent classification accuracy. | $S1_t$+$S2_t > S1_a$+$S2_a$ | Not verified. |
| H3 | Fusion of monotemporal optical and radar images results in better classification accuracy than monotemporal optical or radar images only. | $S1_a$+$S2_a > S1_a$; $S1_a$+$S2_a > S2_a$ | Verified. |
| H4 | Fusion of optical and radar time series results in better classification accuracy than optical time series or radar time series only. | $S1_t$+$S2_t > S1_t$; $S1_t$+$S2_t > S2_t$ | Verified |

# Figures

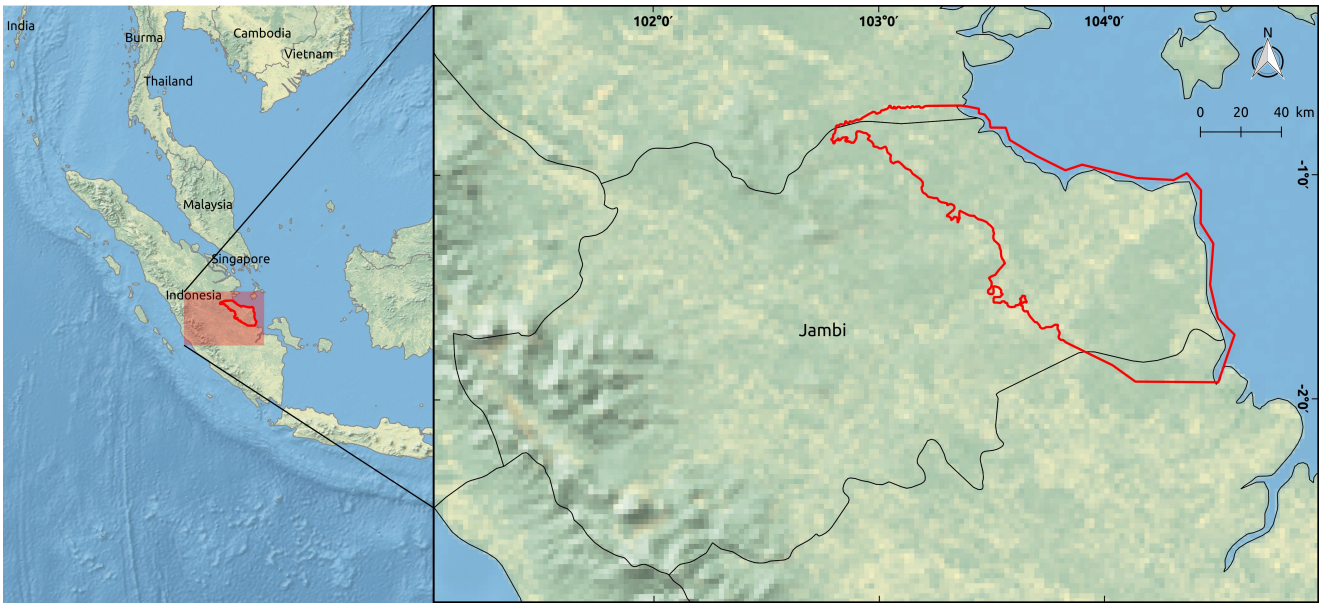


Figure 1: Location of the study area (red lines) in Jambi province, Sumatra (Indonesia). Data: Natural Earth (`https://www.naturalearthdata.com`).

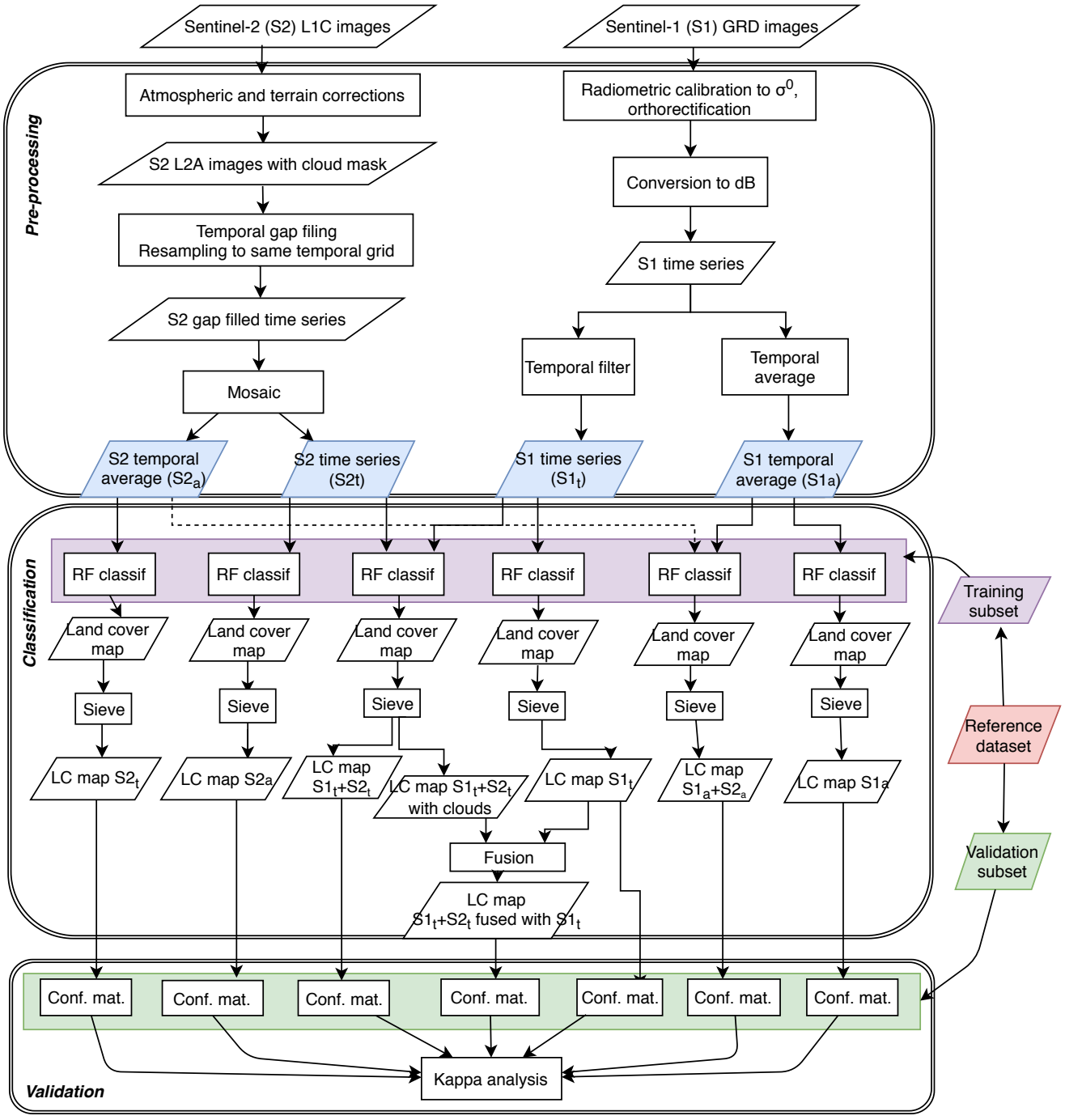


Figure 2: Workflow of the processing and the classification processes. RF classif.: Random Forest classification, LC: land cover, Conf. mat: confusion matrix.

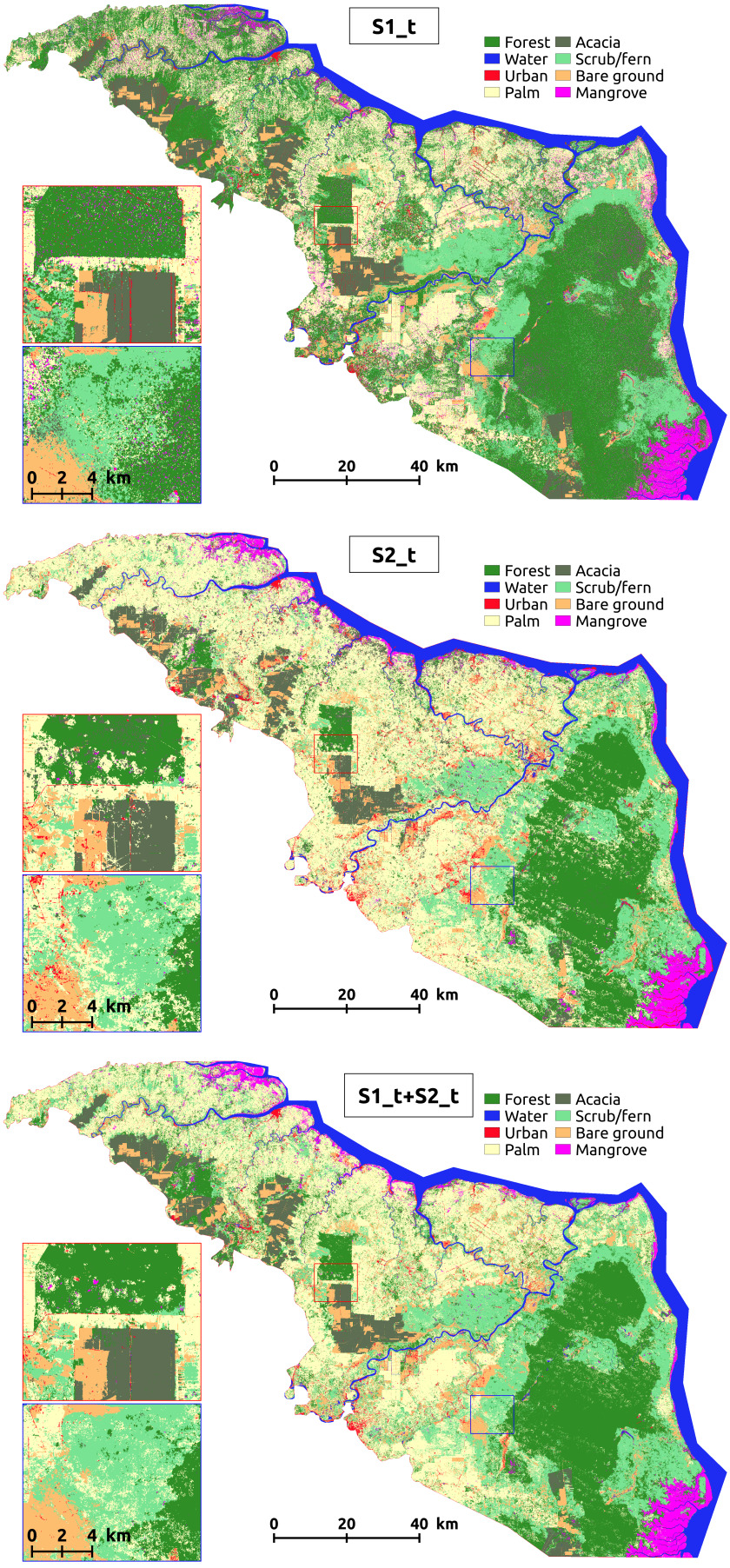


Figure 3: Land cover maps produced from Sentinel-1 time series ($S1_t$, Kappa = 82.9%, top), Sentinel-2 time series ($S2_t$, Kappa = 79.0%, middle) and combination of both ($S1_t$+$S2_t$, Kappa = 88.5%, bottom).

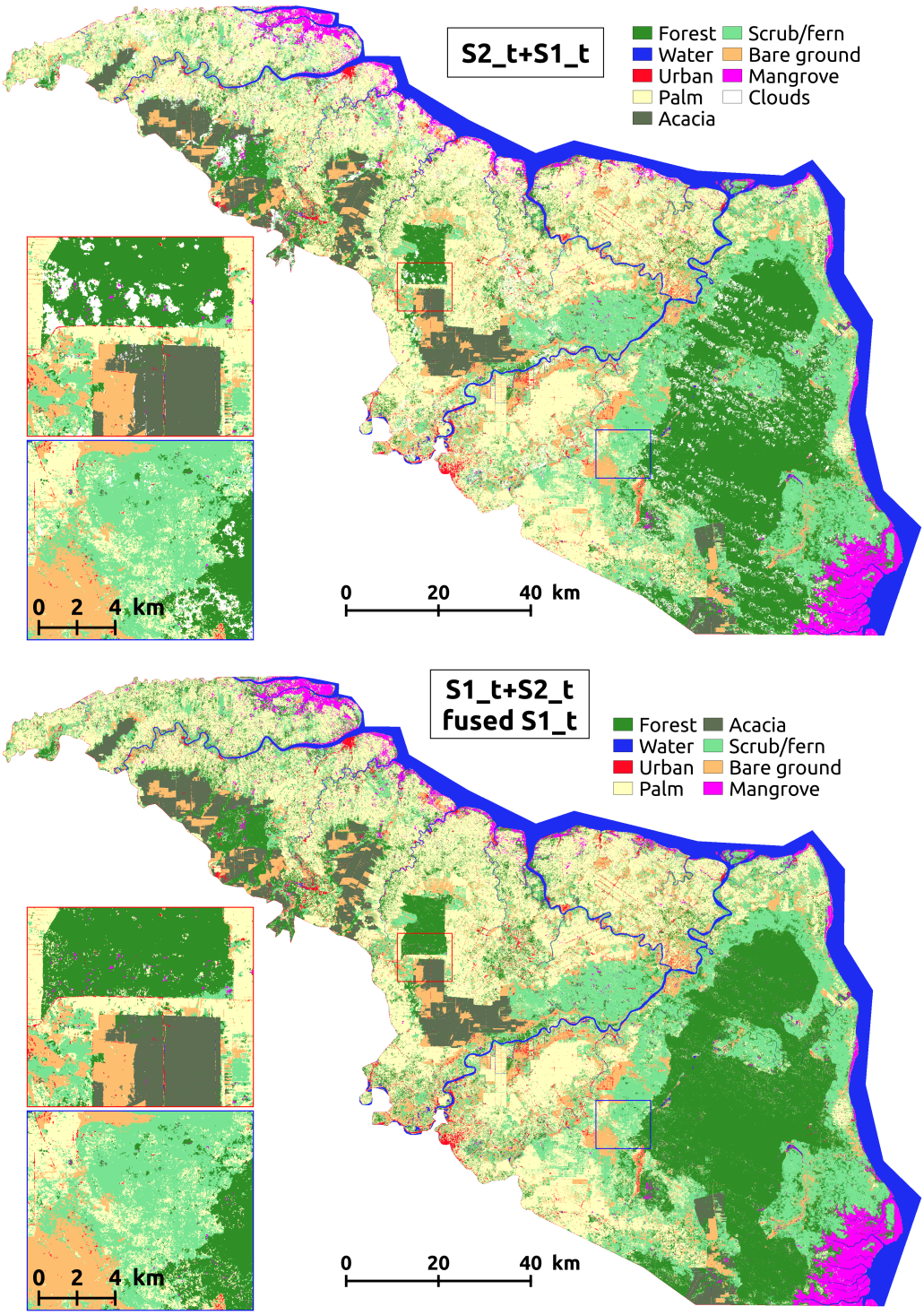


Figure 4: Land cover maps produced from Sentinel-1 & Sentinel-2 time series with cloud class (top) and clouds replaced with Sentinel-1 ($S1_t$) classification ($S1_t$+$S2_t$ fused $S1_t$),Kappa = 89.4, bottom).

# Supporting Information

Table 2: User's accuracy (UA) and producer's accuracy (PA) of each class for each classification's input (values are given in percentage).

| **Class** | **Forest** | | **Water** | | **Urban** | | **Palm** | | **Acacia** | | **Fern** | | **Bare** | | **Mangrove** | |
|---|---|---|---|---|---|---|---|---|---|---|---|---|---|---|---|---|
| **Input** | UA | PA | UA | PA | UA | PA | UA | PA | UA | PA | UA | PA | UA | PA | UA | PA |
| $S1_a$ | 89.5 | 53.8 | 100 | 83.4 | 74.6 | 87.2 | 67.9 | 72.6 | 89.2 | 94.0 | 54.7 | 86.7 | 46.0 | 71.5 | 42.9 | 35.7 |
| $S2_a$ | 90.6 | 82.5 | 97.9 | 79.4 | 36.5 | 93.0 | 56.7 | 67.0 | 77.7 | 73.9 | 91.3 | 91.7 | 62.6 | 87.8 | 87.0 | 85.3 |
| $S1_a$+$S2_a$ | 91.4 | 93.3 | 100 | 83.5 | 63.9 | 97.7 | 77.7 | 81.6 | 91.6 | 88.7 | 91.4 | 92.9 | 68.6 | 86.5 | 95.1 | 85.8 |
| $S1_t$ | 80.8 | 90.3 | 100 | 83.4 | 74.3 | 85.8 | 78.0 | 82.5 | 90.7 | 95.4 | 89.6 | 77.8 | 90.2 | 82.9 | 75.7 | 67.1 |
| $S2_t$ | 93.3 | 81.4 | 99.7 | 79.9 | 36.6 | 96.9 | 55.8 | 85.1 | 83.8 | 81.3 | 94.2 | 83.3 | 68.8 | 81.6 | 91.9 | 88.7 |
| $S1_t$+$S2_t$ | 94.8 | 92.6 | 100 | 83.1 | 65.4 | 98.3 | 74.0 | 92.7 | 91.1 | 93.1 | 93.0 | 90.4 | 82.4 | 84.2 | 97.3 | 87.4 |
| $S1_t$+$S2_t$ fused $S1_t$ | 94.3 | 94.7 | 100 | 83.1 | 71.2 | 98.1 | 79.1 | 90.5 | 91.0 | 93.6 | 93.8 | 92.2 | 81.9 | 85.1 | 95.8 | 87.2 |